

Borane Chemistry

Synthesis of Ammonia Borane Nanoparticles and the Diammoniate of Diborane by Direct Combination of Diborane and Ammonia

Yuanzhou Song^{+, [a]}, Nana Ma^{+, [b]}, Xiaohua Ma,^[a, c] Fang Fang,^[a] Xuenian Chen,^{*, [b]} and Yanhui Guo^{*, [a]}

Abstract: Pure nanoparticle ammonia borane (NH₃BH₃, AB) was first prepared through a solvent-free, ambient-temperature gas-phase combination of B₂H₆ with NH₃. The prepared AB nanoparticle exhibits improved dehydrogenation behavior giving 13.6 wt.% H₂ at the temperature range of 80–175 °C without severe foaming. Ammonia diborane (NH₃BH₂(μ-H)BH₃, AaDB) is proposed as the intermediate in the reaction of B₂H₆ with NH₃ based on theoretical studies. This method can also be used to prepare pure diammoniate of diborane ([H₂B(NH₃)₂][BH₄], DADB) by adjusting the ratio and concentration of B₂H₆ to NH₃.

Ammonia borane (AB), first prepared by Shore in 1955,^[1] has attracted significant attention recently as a solid hydrogen-storage material because of its high hydrogen content (19.6 wt.%), good stability at ambient temperature, and moderate hydrogen-release temperature.^[2] However, AB has severe limitations as a hydrogen-storage material due to some drawbacks including high kinetic barriers,^[2a] the emission of poisoning product (borazine), and material foaming in the dehydrogenation. Over the past few years, a variety of methods such as metal-catalyzing,^[2b, 3] additive-doping,^[4] substitution of the amine hydrogen of AB with metal cations,^[5] and size effects,^[6] have been explored to improve the dehydrogenation of AB. Amongst these methods, size effects have been demonstrated to have a significant impact on the hydrogen-storage performance of the AB nanoparticle loaded in various scaffolds, such as mesoporous silica,^[6a] microporous carbon framework (MCF),^[7] and metal-organic frameworks (MOFs).^[6d] On the

other hand, the pure nanophase of other hydrogen-storage candidates—metal hydrides—demonstrates improved kinetics for reversible hydrogen storage in comparison with the bulk materials.^[8] In considering that scaffolds always carry a mass penalty as a hydrogen-storage method and the nanophase improves dehydrogenation properties of metal hydrides, synthesis and dehydrogenation studies of the pure nanosized AB nanoparticle will be of great significance. We have found conditions under which AB nanoparticles form. Nanoparticle AB exhibits promising dehydrogenation behaviour in comparison with AB formed in the presence of solvent.

The molecular formula of AB (NH₃BH₃) invites the conclusion that AB can be synthesized by direct combination of NH₃ and B₂H₆. However, as first reported by Stock in 1923,^[9] the direct combination yields the diammoniate of diborane (DADB) rather than pure AB in the reaction of B₂H₆ with solid NH₃ (below –100 °C), or in the reaction of liquid NH₃ with gaseous B₂H₆ later reported by Shore, et al.^[10] These results have puzzled the boron chemistry community for decades. Thus, a variety of indirect methods have been developed to synthesize AB. The earliest strategy is by the metathesis reaction of ammonium and borohydride salts in an organic solvent developed by Shore and Parry in 1955,^[11] which was improved by Autrey and Ramachandran.^[11] Newer methods include displacement reactions^[12] and the decomposition of DADB.^[13]

To find a convenient preparation of AB continues to be of practical and theoretical interest. In a recently developed practical synthesis technology, a borane displacement reaction involving tetrahydrofuran borane and liquid NH₃ produces AB,^[10] this reaction also yielded mechanistic insight into the combination of NH₃ with B₂H₆.^[14] Yet, the production of pure nanosized AB has not been reported using the previous methods. Direct combination of NH₃ and B₂H₆ to produce pure AB at ambient temperature remains a desirable but unrealized preparative method.

Meanwhile, DADB the ionic dimer of AB that has also attracted much attention as hydrogen-storage candidate,^[15] remains difficult to synthesize due to the rigorous procedure of the original synthesis and DADB's instability in organic solvents at ambient temperature.^[16] Currently, there is no commercial source of DADB^[10, 16] and the existing preparative methods, the reaction of liquid ammonia with borane,^[9, 10] decomposition of NH₄BH₄,^[17] or ball milling NaBH₄ and NH₄F^[15a, 18] are not suitable for commercialization. The absence of a facile synthesis has become a barrier for the comprehensive study of this ad-

[a] Y. Song,⁺ Prof. X. Ma, Prof. F. Fang, Prof. Y. Guo
Department of Materials Science
Fudan University, Shanghai, 200433 (P. R. China)
E-mail: gyh@fudan.edu.cn

[b] N. Ma,⁺ Prof. X. Chen
School of Chemistry and Chemical Engineering
Henan Normal University, Xinxiang, Henan 453007 (P. R. China)
E-mail: xnchen@htu.edu.cn

[c] Prof. X. Ma
Center of Special Materials and Technology
Fudan University, Shanghai, 200433 (P. R. China)

[†] These authors contributed equally to this work.

Supporting information for this article is available on the WWW under <http://dx.doi.org/10.1002/chem.201600367>.

vanced material, and a practical synthesis method is still urgently needed.

In this study, it is found that solvent-free combination of B_2H_6 with NH_3 can produce both nanosized AB and pure DADB at ambient temperature. Results show that excess B_2H_6 promotes formation of AB, while excess NH_3 leads to formation of DADB. Nanosized AB shows superior dehydrogenation behaviour compared to AB prepared by other methods, improvements that may represent an advantage as investigations of AB as a solid-state hydrogen-storage material continue.

The synthesis of pure AB nanoparticles and pure DADB was realized through the reaction of a B_2H_6 stream with a NH_3 stream in apparatus shown in Figure 1. Ammonia was purified

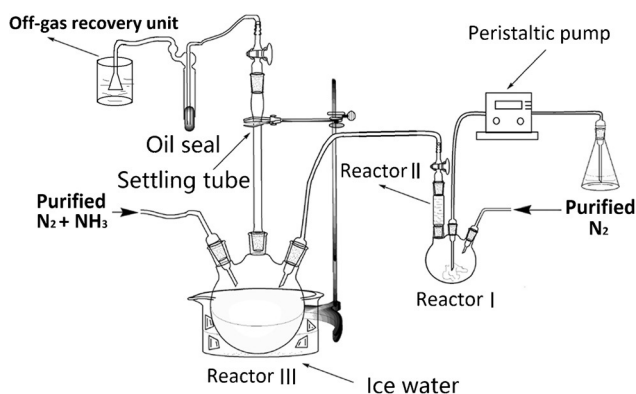
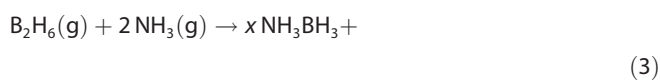
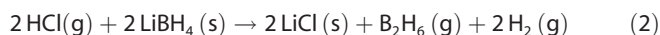
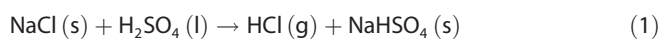


Figure 1. Apparatus for the preparation of AB or DADB by direct combination. Equations (1–3) describe the reactions that occur in Reactors I–III, respectively.

with soda lime and carried on a stream of purified N_2 . B_2H_6 was produced by reacting gaseous HCl (from concentrated H_2SO_4 dripped into dry NaCl using a peristaltic pump [Eq. (1)]), which was carried by purified N_2 through a layer of $LiBH_4$ powder [Eq. (2)].



The absence of Cl^- in the B_2H_6 stream was confirmed by Cl^- titration analysis. The concentration of B_2H_6 was controlled by the H_2SO_4 drop rate. The amount of N_2 diluent controlled the concentration of NH_3 . A detailed experimental procedure is provided in the Supporting Information. Composition of the powdery solid product isolated from Reactor III (500 mL 3-necked flask; Figure 1) was determined by XRD measurements (Figure 2). When reactant ratios were not carefully adjusted both AB and DADB (Figure 2b) were present, which is consistent with previous reports of the reaction of B_2H_6 with liquid NH_3 .^[10] However, it was discovered that pure AB or pure DADB

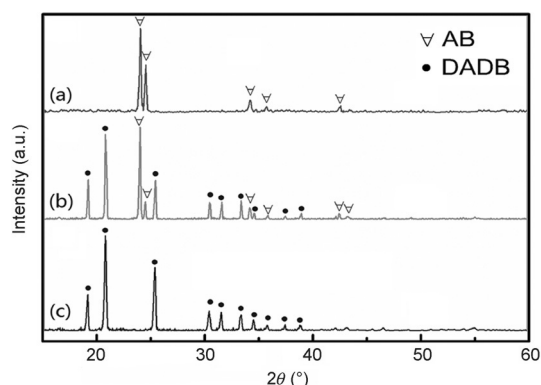


Figure 2. XRD patterns of: a) AB, b) mixture of AB and DADB, and c) DADB.

could be obtained with appropriate adjustment of the ratio of B_2H_6 to NH_3 and their concentrations. Excess B_2H_6 was required to produce pure AB, and excess NH_3 was required to produce pure DADB. Pure AB was synthesized using a B_2H_6/N_2 mixture (15:85 volume ratio) at a flow rate of 10 mL min^{-1} and a NH_3/N_2 mixture (3:97 volume ratio) at a flow rate of 3 mL min^{-1} at ambient temperature. These conditions created a B_2H_6/NH_3 ratio of 17:1. The purity of AB was confirmed by XRD (Figure 2a), FTIR spectroscopy (Figure S3, Supporting Information), NMR (Figure S4, Supporting Information) analyses, and the content of boron element and active hydrogen in the product measured by ICP-AES and active hydrogen analysis^[19] (Table S1, Supporting Information). Typically, around 73 mg of white powder can be collected after 12 h and the theoretical yield of AB, which was calculated according to the amount of NH_3 that flows into Reactor III (Figure) is 83 mg. Therefore, the yield of AB was around 87%. Moreover, the concentration of NH_3 in the NH_3/N_2 mixtures was found to affect the purity of AB. Results show that when the NH_3 concentration was increased, a mixture of DADB and AB formed (Figure S1, Supporting Information).

In contrast to the production of AB, excessive NH_3 environment favors the formation of DADB. Pure DADB was synthesized using a 1:40 ratio of B_2H_6 to NH_3 by mixing B_2H_6/N_2 (4:96 volume ratio, flow rate: 10 mL min^{-1}) and pure NH_3 (flow rate: 4 mL min^{-1}) at ambient temperature. The purity of DADB was confirmed by XRD (Figure 2c), FTIR spectroscopy (Figure S3, Supporting Information), and the content of boron and active hydrogen in DADB^[19] (Table S1, Supporting Information). In this case, the concentration of B_2H_6 will affect the purity of the as-prepared DADB. Higher concentrations of B_2H_6 will lead to the formation of AB impurity (Figure S2, Supporting Information). Typically, around 131 mg DADB can be collected after 12 h compared to the theoretical yield of 402 mg calculated according to the amount of B_2H_6 that is introduced into Reactor III. Therefore, the yield of DADB was around 33%.

It is believed that the influence of concentration is complicated by the inhomogeneity of the B_2H_6/NH_3 ratio in the reactor. Diffusion dynamics may lead to a different ratio of the two starting materials in the center of the flowing gases compared to the bulk material ratio. Therefore, it is difficult to achieve

a consistent reaction environment of stable ratios of B_2H_6 and NH_3 . Presumably inhomogeneity increases the possibility of impurity formation.

Decomposition of the as-prepared DADB and AB was investigated using TGA/MS (Figure S5, Supporting Information), TPD, and DSC (Figure S6, Supporting Information). Dehydrogenation of the as-prepared DADB proceeds in the temperature range of 90–225 °C with significant weight loss (33.6 wt.%) and severe foaming at 300 °C. However, for the as-prepared nanoscale AB, several notable improvements were observed. First, the dehydrogenation temperature of AB prepared in this work is lower than that of AB prepared from solution. Two dehydrogenation peaks were observed by TGA/MS (Figure S7, Supporting Information) and DSC at 101 and 149 °C, compared to 121 and 156 °C for the bulk AB.^[20] Second, weight loss of the as-prepared nanoscale AB (24.9 wt.%) at 300 °C is far below that for AB prepared from solution (around 50 wt.%), suggesting the release of fewer volatile impurities during dehydrogenation (Figure S7, Supporting Information). Finally, no severe material foaming or expansion occurred during the decomposition of the as-prepared AB (Figure S8, Supporting Information). The DSC result suggests that no melting phase transition was present during decomposition of AB (Figure S6, Supporting Information), which indicates that the elimination of foaming may be attributed to new bonds being formed before the melting of AB.^[21] Furthermore, AB prepared by direct combination formed nanoscale particles according to their SEM images (Figure 3 b, around 50 nm), which is consistent with the grain-size

the particle size of AB would affect its hydrogen-storage properties.

Currently, the normal strategy to facilitate size effect is scaffold confinement. Autrey et al. have loaded AB within the mesoporous silica SBA-15, and the confined nanosized AB showed an encouraging one-step dehydrogenation peaking at around 100 °C (heating rate: 1 °C min⁻¹) with little borazine impurity evolution.^[6a] Yao et al. have confined AB into the metal-organic framework (MOF) and the MOF-confined AB produced pure hydrogen peaking at 84 °C (heating rate: 1 °C min⁻¹).^[6d] Although significant dehydrogenation improvement has been achieved using a confinement strategy, the mass penalty of these methods was quite obvious, which made these methods less practical. Pure nanoparticle strategy may be a promising alternative for AB modification due to the comprehensive dehydrogenation improvements without a mass penalty. The enhanced dehydrogenation properties of nanoparticles in our study represents an important advance, further optimization on the particle size or combination of other modification methods may achieve a more efficient AB-based hydrogen-storage system with high hydrogen capacity, practical dehydrogenation temperature, pure hydrogen evolution, and no severe material foaming.

The key intermediate in an early proposed mechanism is ammonia diborane ($NH_3BH_2(\mu-H)BH_3$, AaDB), which was first established in a report by Shore et al. describing the reaction of NH_3 with THF- BH_3 that leads to a mixture of AB and DADB.^[14a] A similar mechanism (Scheme 1) was proposed which is supported by experimental results and computational studies (see the Supporting Information for computational details). Initially NH_3 reacts with B_2H_6 to form AaDB. The reaction is predicted to be exothermic (-3.8 kcal mol⁻¹, Figure S10, Supporting Information) with a calculated activation energy barrier of 8.2 kcal mol⁻¹. Subsequent addition of NH_3 to AaDB at B_a leads to DADB (pathway I) or addition of NH_3 at B_b results in two molecules of AB. The calculated energy profile with structures of reaction complex (RC), transition state (TS), and product complex (PC) is shown in Table S1, Supporting Information. Based on calculated energy barriers (Table 1) formation of AB is

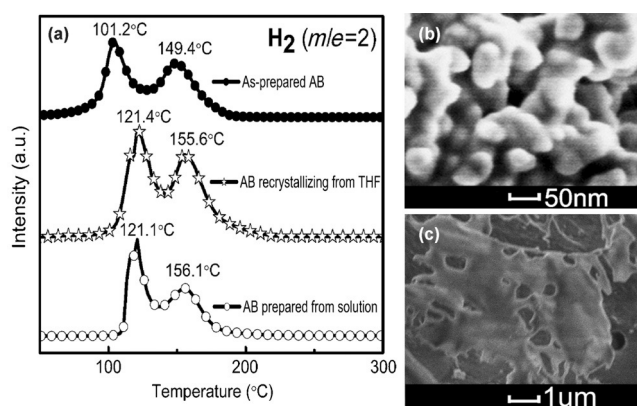
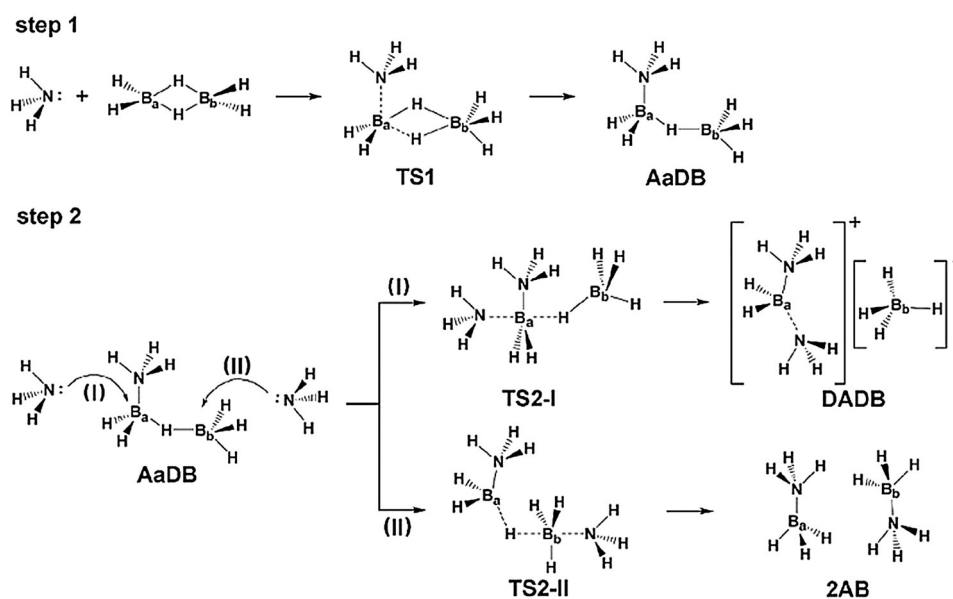


Figure 3. a) MS profiles for the as-prepared nanoscale AB, the as-prepared nanoscale AB resolved in THF and recrystallized from THF, and AB prepared from solution at a heating rate of 5 °C min⁻¹. SEM image for: b) the as-prepared nanoscale AB and c) the as-prepared nanoscale AB resolved in THF and recrystallized from THF.

calculated by the XRD result (around 61 nm). It is supposed that the small size should contribute to the dehydrogenation improvement of AB. To study the size effect, the as-prepared AB nanoparticles were recrystallized in THF to produce AB powder with larger particle size. It shows that apparent increment of AB particles size (Figure 3 c) along with the degradation of its dehydrogenation performance were present after the recrystallization (Figure 3 a). These results may suggest that

Table 1. Calculated free energies (kcal mol⁻¹, at 298 K) of the reaction between NH_3 and AaDB in the presence of AB, B_2H_6 , and NH_3 molecules at the M062X/6-311++G(d,p) level.

	Pathway I			Pathway II		
	RC	TS2-I	DADB	RC	TS2-II	2AB
none	0.0	30.2	-0.8	0.0	13.6	-12.1
one AB	0.0	23.9	-8.0	0.0	12.0	-7.8
two AB	0.0	19.2	-10.6	0.0	10.6	-11.5
three AB	0.0	16.6	-3.3	0.0	12.2	-4.1
four AB	0.0	14.3	-8.0	0.0	11.3	-8.1
one B_2H_6	0.0	27.7	-2.9	0.0	12.6	-5.8
two B_2H_6	0.0	27.3	-4.9	0.0	11.3	-8.5
three B_2H_6	0.0	26.0	-5.0	0.0	9.8	-7.6
one NH_3	0.0	27.7	-3.2	0.0	10.5	-17.1
two NH_3	0.0	24.9	-7.0	0.0	10.8	-5.7
three NH_3	0.0	17.8	-9.2	0.0	10.7	-14.7
four NH_3	0.0	17.1	-10.6	0.0	11.3	-12.6
five NH_3	0.0	16.9	-14.5	0.0	10.6	-12.2



Scheme 1. Proposed mechanism for the formation of AB and DADB by direct combination of NH_3 and B_2H_6 .

strongly favored, $13.6 \text{ kcal mol}^{-1}$ (pathway II) versus $30.2 \text{ kcal mol}^{-1}$ (pathway I). However, while pure AB has been obtained, mixtures of AB and DADB (Figure 2b) and pure DADB have been obtained depending upon reaction conditions. Factors not represented in the mechanism must be involved.

Shore et al. have reported that dihydrogen bonds between AaDB and AB play a crucial role in DADB formation in the solution reaction of NH_3 with $\text{THF}\cdot\text{BH}_3$.^[14a] In the present case, dihydrogen bond interactions between AaDB and AB were introduced resulting in a dramatic decrease ($6.3 \text{ kcal mol}^{-1}$) in the calculated activation energy of pathway I, but little change for pathway II (Table 1). TS structures are shown in Figures S12 and S13, Supporting Information. More dihydrogen bonds from the more complexed AB slow the calculated activation barrier further. When four AB molecules are present, the predicted activation energy for pathway I is $14.3 \text{ kcal mol}^{-1}$, comparable to the $11.3 \text{ kcal mol}^{-1}$ barrier calculated for the pathway II. It is also observed that DADB formation is calculated to be more exothermic in the presence of AB.

When B_2H_6 is in excess, AaDB forms dihydrogen bond $\text{N}\cdots\text{H}\cdots\text{B}$ and homopolar dihydrogen bond $\text{B}\cdots\text{H}\cdots\text{B}$ ^[22] with excess B_2H_6 rather than with the small amount of AB present. Energy barriers of pathways I and II were calculated in the presence of one, two, and three B_2H_6 molecules (Table 1) and the TS structures are provided in Figures S14 and S15, Supporting Information. The calculated activation energy barriers of both pathways I and II were reduced generally with the formation of dihydrogen bonds. When three B_2H_6 molecules were considered to form dihydrogen bonds with AaDB, the energy barrier for pathway I ($26.0 \text{ kcal mol}^{-1}$) was significantly higher than the barrier of pathway II ($9.8 \text{ kcal mol}^{-1}$) (Table 1). This is probably the reason for the formation of pure AB in the presence of excess B_2H_6 .

At higher NH_3 concentrations, dihydrogen bonds and hydrogen bonds ($\text{N}\cdots\text{H}\cdots\text{N}$) involving AaDB can be expected. In the

presence of one NH_3 molecule, the calculated activation energy barrier for AB formation was reduced to $10.5 \text{ kcal mol}^{-1}$, much lower than the barrier for DADB formation ($27.7 \text{ kcal mol}^{-1}$) (Table 1, TS structures are shown in Figures S16 and S17, Supporting Information). As the proportion of NH_3 is increased, the activation energy barrier of AB formation changed little but the barrier to DADB formation decreased significantly. However, these calculations do not account for the formation of pure DADB since the energy barrier to DADB formation is consistently higher than for AB formation. Therefore, other factors such as dynamic influence might play important roles in this reaction.

In the transition-state TS2-I of the pathway I, a six-membered $\text{B}_a\text{--N}\cdots\text{H}\cdots\text{B}_b\text{--H}$ ring is formed through dihydrogen bonding interactions. The formation of a dihydrogen bond and the six-membered ring are considered as key factors in this step. In order to confirm their important roles, trimethylamine was used to react with B_2H_6 in which no dihydrogen bond could be formed after protonic hydrogen had been replaced by a methyl group. Experimental results indicate that in either trimethylamine or B_2H_6 excess, only pure trimethylamine borane (Me_3NBH_3 , TMB) was formed. This observation indirectly proves that the formation of the dihydrogen bond and six-membered ring may play key roles in the formation of DADB.

In summary, effective synthesis of the pure nanoscale of AB and pure DADB has been developed by the gas-phase combination of NH_3 and B_2H_6 . The mechanistic implications of the dependence of product formation on relative ratio and concentration of reagents have been analysed. The dehydrogenation properties of pure AB and DADB have been characterized with encouraging results. Pure AB yields $0.068 \text{ mol H}_2/\text{g}$ (around 13.6 wt.%) in the temperature range $80\text{--}175^\circ\text{C}$ without severe foaming, behaviour that is attributed to its nanoparticle size. This work not only provides a convenient procedure for preparation of pure nanoscale AB and pure DADB, but

also shed light on the relationship of compound properties, particle size and its synthetic method, which will benefit a wide range of readers.

Experimental Section

General

NH₃BH₃ (97%, United boron (Zhengzhou) S&T LLC, China) was used as received. LiBH₄ (95%, Sigma-Aldrich, USA) and NaCl (Sino-pharm Chemical Reagent Co., Ltd, China) were ball milled for 1 h before use. NH₃ gas (Alfa Aesar, China) was purified by bubbling through soda lime before use. THF (98%, Sinopharm Chemical Reagent Co., Ltd, China) was dried over sodium/benzophenone and distilled prior to use. All samples, except H₂SO₄ (95–98%, Zhitang Chemical Co., Ltd, China), were handled in a nitrogen-filled glove box that kept water and oxygen concentrations below 1 ppm during operation. The flow rates of N₂ and NH₃ were controlled by gauges (LZB-2 6–60ML/MIN, Yuzhaoweichuang Flow Gauge CO., Ltd, China) and peristaltic pump (BS100–1AQ, BAODING SIGNAL FLUID TECHNOLOGY CO., Ltd, China). The flow rate of B₂H₆/N₂ mixture and NH₃/N₂ mixture were measured by the flowmeter (FS4001, Siargo Ltd., America).

Notice, B₂H₆ and NH₃ are extremely toxic gas and should therefore only be handled in fumehood with ventilation. Off-gas should be bubbled into 5% ammonia solution for security.

All the calculations were performed using Gaussian 09 program. The structures were fully optimized at the M062X/6–311 + G(d,p) level in gas phase. M062X functional was proved to be very accurate for reproducing the thermodynamic data, barrier heights, isomerization energies. The vibrational frequency was calculated at the same level to determine whether it is an equilibrium structure or a transition state (TS). The corresponding normal mode for the imaginary vibrational frequency then suggested the related reactant and product for that transition state. The Gibbs free energy (ΔG , kcal mol⁻¹ at 298 K) barriers can be used to discuss the reaction between NH₃ and B₂H₆ to produce DADB and AB. The Cartesian coordinates and vibrational frequencies of the studied models are provided in this Supporting Information. The active hydrogen was determined by hydrolysis of the sample in 2 M-hydrochloric acid within a sealed bulb. The amount of hydrogen released during the hydrolysis was calculated by the pressure variation of the system. Inductively coupled plasma-atomic emission spectrometry (ICP-AES) measurements were conducted using Hitachi Limited P-4010. Before the ICP-AES measurements, samples were dissolved in 5 wt.% hydrochloric acid to produce a solution with a concentration of 50–100 mg L⁻¹. Powder XRD patterns were obtained by D8 Advance Bruker AXS with Cu_{K α} radiation (1600 W). During the XRD measurement, samples were mounted in a glove box, and covered by an amorphous polymer tape to avoid oxidation. Temperature-programmed desorption (TPD) and volumetric-release measurements were carried out using a semiautomatic Sievert's apparatus, connected with a reactor filled with a sample (typical weight \approx 30 mg) under nitrogen atmosphere (\approx 1 bar). The sample was heated from 25 to 300 °C at a rate of 5 °C min⁻¹. The ¹¹B NMR spectroscopy experiments were recorded using a Bruker DMX (500 MHz, 11.7 T) at room temperature. All samples were dissolved in [D₂]THF. Thermogravimetric analysis and mass spectrometry (TGA-MS) measurements were conducted from 30 to 300 °C under argon at a heating rate of 5 °C min⁻¹ using TGA Q500 equipped with a quadrupole mass spectrometer for the analysis of the evolved gas. The targeted evolving gas monitored by MS was H₂ ($m/e=2$). Differential Scanning Calorimetry (DSC) results were

collected using a TA Q100. Samples were heated from room temperature to 300 °C at a heating rate of 5 °C min⁻¹ under nitrogen. FTIR (Netzch Nicolet Is10) analyses were conducted using the KBr-pellet method and recorded in the range 500 to 4000 cm⁻¹. SEM images were collected on SUPERSCAN SSX-550. Dried samples with an ultrathin coating of electrically-conducting material were used for observation.

Acknowledgements

This work was financially supported by National Natural Science Foundation of China (51201035, 51471052, U1201241, 21371051), the Doctoral Program of Higher Education of China (20110071120008) and Key Laboratory of Advanced Energy Storage Materials of Guangdong Province. The authors are grateful to Prof. T. Evans for very valuable comments.

Keywords: ammonia borane · borane chemistry · diammoniate of diborane · hydrogen storage · nanotechnology

- [1] S. G. Shore, R. W. Parry, *J. Am. Chem. Soc.* **1955**, *77*, 6084–6085.
- [2] a) G. Wolf, J. Baumann, F. Baitalow, F. P. Hoffmann, *Thermochim. Acta* **2000**, *343*, 19–25; b) J.-M. Yan, X.-B. Zhang, S. Han, H. Shioyama, Q. Xu, *Angew. Chem. Int. Ed.* **2008**, *47*, 2287–2289; *Angew. Chem.* **2008**, *120*, 2319–2321; c) T. B. Marder, *Angew. Chem. Int. Ed.* **2007**, *46*, 8116–8118; *Angew. Chem.* **2007**, *119*, 8262–8264; d) U. Eberle, M. Felderhoff, F. Schueth, *Angew. Chem. Int. Ed.* **2009**, *48*, 6608–6630; *Angew. Chem.* **2009**, *121*, 6732–6757; e) G. R. Whittell, I. Manners, *Angew. Chem. Int. Ed.* **2011**, *50*, 10288–10289; *Angew. Chem.* **2011**, *123*, 10470–10472; f) G. R. Whittell, I. Manners, *Angew. Chem.* **2011**, *123*, 10470–10472.
- [3] a) P.-Z. Li, A. Aijaz, Q. Xu, *Angew. Chem. Int. Ed.* **2012**, *51*, 6753–6756; *Angew. Chem.* **2012**, *124*, 6857–6860; b) G. Alcaraz, S. Sabo-Etienne, *Angew. Chem. Int. Ed.* **2010**, *49*, 7170–7179; *Angew. Chem.* **2010**, *122*, 7326–7335; c) G. Alcaraz, S. Sabo-Etienne, *Angew. Chem.* **2010**, *122*, 7326–7335.
- [4] D. J. Heldebrant, A. Karkamkar, N. J. Hess, M. Bowden, S. Rassat, F. Zheng, K. Rappe, T. Autrey, *Chem. Mater.* **2008**, *20*, 5332–5336.
- [5] H. V. K. Diyabalanage, R. P. Shrestha, T. A. Semelsberger, B. L. Scott, M. E. Bowden, B. L. Davis, A. K. Burrell, *Angew. Chem. Int. Ed.* **2007**, *46*, 8995–8997; *Angew. Chem.* **2007**, *119*, 9153–9155.
- [6] a) A. Gutowska, L. Li, Y. Shin, C. M. Wang, X. S. Li, J. C. Linehan, R. S. Smith, B. D. Kay, B. Schmid, W. Shaw, M. Gutowski, T. Autrey, *Angew. Chem. Int. Ed.* **2005**, *44*, 3578–3582; b) A. Feaver, S. Sepehri, P. Shamberger, A. Stowe, T. Autrey, G. Cao, *J. Phys. Chem. B* **2007**, *111*, 7469–7472; c) Z. Tang, X. Chen, H. Chen, L. Wu, X. Yu, *Angew. Chem. Int. Ed.* **2013**, *52*, 5832–5835; *Angew. Chem.* **2013**, *125*, 5944–5947; d) Z. Li, G. Zhu, G. Lu, S. Qiu, X. Yao, *J. Am. Chem. Soc.* **2010**, *132*, 1490–1491.
- [7] L. Li, X. Yao, C. Sun, A. Du, L. Cheng, Z. Zhu, C. Yu, J. Zou, S. C. Smith, P. Wang, H.-M. Cheng, R. L. Frost, G. Q. Lu, *Adv. Funct. Mater.* **2009**, *19*, 265–271.
- [8] H. Fujii, S. Orimo, *Physica B-Condensed Matter* **2003**, *328*, 77–80.
- [9] a) A. Stock, E. Kuss, *Ber. Deut. Chem. Ges.* **1923**, *56*, 789–808; b) H. T. Schlesinger, A. B. Burg, *J. Am. Chem. Soc.* **1938**, *60*, 290–299.
- [10] S. G. Shore, K. W. Boddeker, *Inorg. Chem.* **1964**, *3*, 914–915.
- [11] a) P. V. Ramachandran, P. D. Gagare, *Inorg. Chem.* **2007**, *46*, 7810–7817; b) D. J. Heldebrant, A. Karkamkar, J. C. Linehan, T. Autrey, *Energy Environ. Sci.* **2008**, *1*, 156–160.
- [12] X. Chen, X. Bao, B. Billet, S. G. Shore, J.-C. Zhao, *Chem. Eur. J.* **2012**, *18*, 11994–11999.
- [13] E. Mayer, *Inorg. Chem.* **1973**, *12*, 1954–1955.
- [14] a) X. Chen, X. Bao, J.-C. Zhao, S. G. Shore, *J. Am. Chem. Soc.* **2011**, *133*, 14172–14175; b) X. Chen, J.-C. Zhao, S. G. Shore, *Acc. Chem. Res.* **2013**, *46*, 2666–2675.

- [15] a) Z. Fang, J. Luo, X. Kang, H. Xia, S. Wang, W. Wen, X. Zhou, P. Wang, *Phys. Chem. Chem. Phys.* **2011**, *13*, 7508–7513; b) M. Bowden, D. J. Heldebrant, A. Karkamkar, T. Proffen, G. K. Schenter, T. Autrey, *Chem. Commun.* **2010**, *46*, 8564–8566.
- [16] H. K. Lingam, X. Chen, J.-C. Zhao, S. G. Shore, *Chem. Eur. J.* **2012**, *18*, 3490–3492.
- [17] A. Karkamkar, S. M. Kathmann, G. K. Schenter, D. J. Heldebrant, N. Hess, M. Gutowski, T. Autrey, *Chem. Mater.* **2009**, *21*, 4356–4358.
- [18] W. J. Shaw, J. C. Linehan, N. K. Szymczak, D. J. Heldebrant, C. Yonker, D. M. Camaioni, R. T. Baker, T. Autrey, *Angew. Chem. Int. Ed.* **2008**, *47*, 7493–7496; *Angew. Chem.* **2008**, *120*, 7603–7606.
- [19] P. H. Bird, M. G. H. Wallbridge, *J. Chem. Soc.* **1965**, 3923–3928.
- [20] a) A. Staubitz, A. P. M. Robertson, I. Manners, *Chem. Rev.* **2010**, *110*, 4079–4124; b) S. F. Li, Y. H. Guo, W. W. Sun, D. L. Sun, X. B. Yu, *J. Phys. Chem. C* **2010**, *114*, 21885–21890.
- [21] T. He, Z. Xiong, G. Wu, H. Chu, C. Wu, T. Zhang, P. Chen, *Chem. Mater.* **2009**, *21*, 2315–2318.
- [22] a) D. J. Wolstenholme, J. T. Titah, F. N. Che, K. T. Trabolsee, J. Flogeras, G. S. McGrady, *J. Am. Chem. Soc.* **2011**, *133*, 16598–16604; b) D. J. Wolstenholme, K. T. Trabolsee, Y. Hua, L. A. Calhoun, G. S. McGrady, *Chem. Commun.* **2012**, *48*, 2597–2599.

Received: January 26, 2016

Published online on March 21, 2016